RSC Advances

PAPER

View Article Online
View Journal | View Issue

Cite this: *RSC Adv.*, 2020, **10**, 43066

Tuning the structural properties of cadmium–aluminum layered double hydroxide for enhanced photocatalytic dye degradation†

Daniel Saliba,‡[a] Salah Eddin El Jamal,‡[b] Antranik Jonderian,[a] Manal Ammar,[b] Mohamad Hmadeh *[b] and Mazen Al-Ghoul *[ab]

Received 18th September 2020
Accepted 19th November 2020

DOI: 10.1039/d0ra08006c

rsc.li/rsc-advances

The distinctive layered structure, chemical stability and tunability of layered double hydroxides (LDHs) have led to extensive investigations in various areas of photocatalysis, including photocatalytic water splitting, carbon dioxide photoreduction, and degradation of organic pollutants. Here, a series of visible light active cadmium–aluminum layered double hydroxides (CdAl LDHs) with various Cd^{2+} : Al^{3+} ratios is synthesized *via* the reaction-diffusion framework (RDF) leading thereby to a hierarchal spherical structure of the LDH. The aim of this study is to develop an optimal CdAl LDH photocatalyst that is activated by solar light irradiation and tested for methylene blue (MB) degradation. The structural and physicochemical properties of the synthesized materials are determined by several imaging and spectroscopic techniques. The photocatalytic study reveals a strong dependence of the photocatalytic activity of the CdAl LDH on the cationic ratio with an optimal performance at a ratio Cd^{2+} : Al^{3+} equal to 3 : 1. A mechanism is proposed whereby the activity is ascribed to the formation of intermediate reactive oxidative species (ROS) during the photodegradation reactions and scrutinised by invoking different ROS quenchers and corroborated by density functional theory (DFT) calculations.

A. Introduction

Increasing attention has been recently paid to semiconductor photocatalysts, such as metal sulfides and metal oxides, due to their importance in industrial applications such as solar light conversion and heterogenous photocatalysis.[1–5] The photoactivity of these materials is highly dependent on the recombination rate of the electron–hole pairs which are generated upon irradiation with light having an energy equal to or higher than the semiconductor band gap.[5] However, most of these photocatalysts present one or more critical drawbacks such as: (i) activation under UV-light due to their large band gap, (ii) containing noble metals dopants to enhance their photoactivity, (iii) having a high recombination rate of electrons and holes, (iv) showing low photochemical stability under irradiation, (v) low porosity, poor adsorption capacity, and difficulty in their recycling.[6–10] Recently, layered double hydroxides (LDHs) have emerged as one of the most promising alternatives for many oxides-, and sulfides-based photocatalysts due to their crystalline layered structure, absorption in the visible region, low manufacturing cost and ease of synthesis.[11,12]

LDHs are a group of 2D layered anionic clays with the general chemical formula $[M(II)_{(1-x)}M(III)_x(OH)_2]^{x+}(X_{x/n}{}^{n-})\cdot mH_2O$, where M(II) and M(III) are the metal cations with x as the cationic ratio while X^{n-} is an intercalator anion.[13,14] The structure of LDH resembles that of brucite-like structures where the divalent metal cations are octahedrally coordinated by hydroxide anions.[15] These octahedral units (MO_6) share edges to form infinite sheets which affect the photocatalytic properties of LDHs.[15] The trivalent and divalent metal cations found in LDHs mainly belong to the third and fourth period of the periodic table.[16] The presence of two different metal cations renders LDHs as doped semiconductors with interesting photocatalytic and photophysical properties.[16] Also, these transition metals octahedrons are distributed in a uniform manner within the hydroxide layers which favors the electron transfer process over the recombination of electrons and holes.[17] In addition, the presence of hydroxyl groups on the surface of the brucite-like sheets favors the $HO^{\bullet}$ radicals formation, which are one of the main reactive oxygen species used in the photocatalytic processes.[18] Moreover, the existence of an interlayer spacing plays an important role in the separation and diffusion of the charge carriers photogenerated by the MO_6 octahedrons.[19] All these properties render LDHs a compelling choice as effective

[a]*Department of Chemistry, McGill University, 801 Sherbrooke St W, Montreal, Quebec, H3A 0B8, Canada*

[b]*Department of Chemistry, American University of Beirut, P. O. Box 11-0236, Riad El-Solh, 1107 2020, Beirut, Lebanon. E-mail: mazen.ghoul@aub.edu.lb; mohamad.hmadeh@aub.edu.lb; Fax: +961 1 365217; Tel: +961 1 350000*

† Electronic supplementary information (ESI) available: Characterization and optical properties of CdAl LDHs. Full spectra of photocatalytic activity of CdAl LDH. Chemical stability of CdAl LDHs after photodegradation. See DOI: 10.1039/d0ra08006c

‡ These authors contributed equally.

photocatalysts in the field of photocatalytic water splitting, carbon dioxide reduction, and degradation of organic pollutants.[20–22] Recently, the photocatalytic performance of LDHs has extended from simple bicationic LDHs into more complex species such as multicationic-phased LDHs, core–shell structured LDHs,[23] doped LDHs,[24] LDHs derived mixed metal oxides,[25] and intercalated LDHs.[26] These complex LDHs offered control over many factors that affect the photocatalytic performance of these structures, including band gap, surface area, and exposed catalytic sites. In most cases, the photocatalytic efficiency relied on the degradation of organic pollutants (rhodamine, methylene blue and methyl orange).[27] Bicationic LDHs revealed degradation efficiencies that can range from 30% to almost 100% with an organic dye concentration ranging from 5 mg L^{-1} to 10 mg L^{-1}.[27–32] Most of the high photodegradation efficiencies (>70%) that were reported for bicationic LDHs were performed in the presence of hydrogen peroxide that enhances the activity of the LDHs mainly due to the formation of hydroxyl radicals.

Different methods have been used to synthesize various LDHs and include ion-exchange synthesis,[14] calcination–rehydration (reconstruction method),[33] microwave assisted synthesis,[34] urea process synthesis,[14] hydrothermal synthesis,[35] and co-precipitation.[35] Synthesis *via* co-precipitation is the most widely used technique to synthesize LDHs. It consists of adding a sodium hydroxide solution into a metal solution mixture, followed by thermal treatment and aging.[14] Recently, our group reported the synthesis of visible light active CdAl LDHs[20] using the reaction-diffusion framework (RDF) method.[36] RDF is advantageous for multiple reasons. It is carried out under facile conditions compared to the co-precipitation method where control of the pH of the medium, thermal treatment, and aging of the LDH are required. Also, it exploits the supersaturation spatial gradient along the reactor that translates into a particle size distribution that can range from the nanometer to the micrometer scales in the same reactor. Moreover, the hydrogel matrix assists the self-assembly of the LDH into unique morphologies that are difficult to obtain using other preparation methods.[13,20,37]

It was shown that CdAl LDH showed a promising performance in the photodegradation of CO_2 using solar light. However, to our knowledge, the potential application of CdAl LDH in aqueous heterogenous photocatalysis has not been investigated.

In this study, we make use of the unique morphology of the reported CdAl LDH that consists of inter-connected individual nano-sheets which assemble into a hierarchical flowery-like spheres with full control over their size which is of particular interest in the field of photocatalysis.[6] The 2D nanosheets of CdAl LDH can be superior to the prevalent platelet-like LDHs as they can provide an efficient electronic transfer resulting in long-lived charge carriers. Therefore, we explore the photoactivity of CdAl LDH as a catalyst for dye degradation in water. Methylene blue is selected as a model dye since it is a commonly used dye in many biological and pharmaceutical applications.

Herein, we demonstrate that CdAl LDHs can be used in the photodegradation of methylene blue using visible light irradiation and in the absence of hydrogen peroxide unlike previous reports where H_2O_2 was necessary for the degradation process.[38–40] Also, we show the dependence of the photocatalytic activity of the CdAl LDHs on its cationic ratio where the Cd^{2+} played an indispensable role. The characterization of the CdAl LDHs with three different cationic ratios is performed using X-ray diffraction (XRD), thermal gravimetric analysis (TGA), scanning electron microscopy (SEM), nitrogen adsorption and UV-Vis spectroscopy. The role of each of the reactive oxygen species in the photocatalytic degradation of methylene blue is investigated by using different scavengers. Finally, the experimental studies are coupled with DFT calculations to assist in understanding the underlying degradation mechanism.

B. Experimental

1. Materials

Aluminum chloride, isopropanol and methylene blue were supplied by ACROS. Sodium hydroxide pellets, benzoquinone and EDTA were provided by Sigma-Aldrich. Cadmium chloride was purchased from RIEDEL-DE HAEN while LB agar (Lennox) was provided by Conda. All chemicals were directly used without any further purification.

2. Synthesis of CdAl LDH

CdAl LDH was prepared using a reaction-diffusion framework. Typically, the required mass of agar gel (1% w/w) was weighed and added to distilled water. The mixture was heated (*ca.* 85 °C) and stirred until total dissolution of the gel. Next, the needed amount of cadmium and aluminum chloride salts were added so that the total metal salts concentration is 0.1 M. Then, the hot mixture was transferred into a test tube (20 × 150 mm) and left at room temperature to polymerize. After 3 hours, a 2 M sodium hydroxide solution was added on top of the gel matrix and left for 2 days to allow the formation of the CdAl LDH photocatalyst along with a brucite band resulting from the polymorphic transformation of the LDH into a brucite-like compound.[20] The LDH band was extracted and washed with hot water (*ca.* 95 °C) under continuous stirring until the complete dissolution of the agar network. Further washing with distilled water was performed to ensure that no cationic metals are adsorbed on the LDH surface. Then, the mixture was centrifuged for 5 min, the precipitate was isolated, freeze dried for 12 hours and re-collected for analysis. The cationic ratio of the CdAl LDH was varied between 0.25 and 0.33, as it was mentioned in a previous report.[37] Briefly, three different preparations were performed where the Cd^{2+} : Al^{3+} ratio in the initial mixture was equal to 1 : 1, 2 : 1 and 3 : 1, these percentages resulted in a final LDH cationic ratio of $x = 0.33$, $x = 0.28$ and $x = 0.25$, respectively. Energy-dispersive X-ray spectroscopy was applied to confirm the formation of CdAl LDH with the desired cationic ratios (Fig. S1†).

3. Solid characterization

The XRD patterns of CdAl LDHs having different cationic ratios were recorded at room temperature with a Bruker D8 Advance

diffractometer using a Cu-Kα radiation source ($\lambda = 0.1541$ nm), an accelerating voltage of 40 mA and 40 kV and a step size of 0.02°. The thermal analysis was carried out using a TG 209 F1 Iris (Netzsch, Germany) thermo-gravimetric analyzer under nitrogen atmosphere with a heating rate of 5 °C min^{-1}. The N_2 adsorption–desorption isotherms were recorded on a Micromeritics ASAP 2420 analyzer. The UV-Vis analyses were obtained using Thermo Scientific Evolution Array UV-visible spectrophotometer where the diffuse reflectance spectra were obtained using a JASCO V-570 UV/Vis/NIR spectrophotometer. The ^{27}Al solid-state nuclear magnetic resonance (ssNMR) spectra were recorded by collecting 1024 transients at a resonance frequency of 104.27 MHz with 12k spinning rate using a Double Resonance Broadband BB/^{1}H 4 mm Bruker cross polarization magic angle spinning (CP/MAS) probe. The samples for scanning electron microscopy (SEM) were prepared by suspending the solid particles in deionized water, sonicating them for 10 min and coating a dilute suspension on a carbon tape. The SEM images and EDX measurement were taken using TESCAN MIRA electron microscope. The internal structure of the particles was imaged using Titan CT (FEI Company) operating at 300 kV equipped with a 4k × 4k CCD camera (Gatan). The 3D tomographic reconstruction was attained using the Xplore 3D tomography software. The LDH microspheres were tilted from −65° to +65° and imaged at 2° intervals between 0° and 50° and 1° interval between 50° and 65°. The tilt series were aligned, and tomograms were obtained using IMOD. 3D rendering models were generated with the segmentation tools implemented in Avizo. The near-surface of the as synthesized LDH were characterized by X-ray photoelectron spectroscopy (XPS) using a Thermo Scientific K-alpha photoelectron spectrometer and a micro-focused monochromatic Al Kα radiation. The acquired spectra were analyzed using Advantage software.

4. Photocatalytic experiments

The photocatalytic activity of all LDHs was investigated by degradation of aqueous methylene blue, acting as a model pollutant of water, under visible light illumination. The photodegradation experiments were carried out in a photo-reactor, equipped with a 100 W xenon lamp, an AM 1.5 optical filter, a magnetic stirrer and a jacketed beaker to maintain a constant temperature, placed 20 cm away from the light source, containing 0.6 g L^{-1} of catalyst (CdAl LDH) and 7.5 mg L^{-1} of methylene blue. Prior to irradiation, the catalyst/organic dye mixture was stirred in the dark for 45 min to reach the adsorption equilibrium and then exposed to the light source. Samples were taken at time intervals and the residual methylene blue absorption was detected by a spectrophotometer.

5. Computational methods

The bulk crystal structure of CdAl LDH was constructed starting from that of MgAl LDH crystal structure (COD 2102792).[41] $R\bar{3}m$ space group was retained while the magnesium cations and interlayer carbonate anions were replaced by cadmium and chloride ions, respectively. All the DFT calculations were performed with plane-wave basis sets. The Perdew–Burke–Ernzerhof (PBE) function within a generalized gradient approximation (GGA) was used to describe the exchange and correlation terms of the valence electrons. Ultrasoft pseudopotentials were employed to model the electron–ion interactions. Monkhorst-Pack grid was used for the Brillouin zone sampling with 0.04 A^{-1} separation. Both the ionic positions and the lattice parameters were fully optimized using Broyden–Fletcher–Goldfarb–Shanno (BFGS) scheme with a convergence tolerance of 5.0×10^{-6} eV per atom for energy and 1.0×10^{-2} eV $Å^{-1}$ for residual forces. The band structure and density of states (DOS) of the relaxed structures were also calculated using the same computational conditions as described above.

C. Results and discussion

1. CdAl LDH characterization

The PXRD patterns of the extracted yellow precipitates, having different cationic ratios, (Fig. 1), reveals four peaks at around 11° (003), 22° (006), 34° (009), and 38° (015) characteristic of an LDH phase with a rhombohedral symmetry.[13] The interlayer spacing ($d_{(003)}$) is determined using the main Bragg reflection peak located at around 11°. CdAl LDHs with cationic ratios of 0.33, 0.28 and 0.25 reveals a spacing of 7.69 Å, 7.74 Å and 7.78 Å, respectively. As the cationic ratio of LDH increases, the number of trivalent cations in the brucite-like sheets increases, requiring more interlayer anions to restore the electroneutrality of the structure. Thus, the overall electrostatic attraction between the brucite-like sheets increases, causing the slight decrease in the interlayer spacing.

The transmission electron microscopy (TEM) images reveal a spherical structure of CdAl LDH particles (Fig. S2(A)†). Fig. S2(B and C)† presents a TEM image of one piece of a CdAl LDH platelet and its corresponding selected area electron diffraction (SAED) pattern that reveals two faint rings corresponding to the (003) and (006) inter-layer periodicity of LDH confirming its layered structure. The obtention of a high resolution TEM image was challenging since the LDH structure is very sensitive to the electron beam illumination and is rapidly

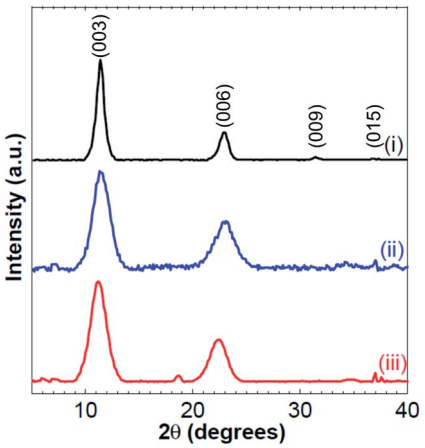

Fig. 1 PXRD patterns of CdAl LDH having a cationic ratio of $x = 0.33$ (i), $x = 0.28$ (ii) and $x = 0.25$ (iii).

damaged. The XRD and the SAED patterns gives similar $d_{(003)}$ and $d_{(006)}$ inter-planar distances.

The TGA curves of CdAl LDHs, having different ratios, show four main mass losses (Fig. S3†). The first mass loss occurring from ambient temperature to approximately 100 °C is ascribed for the elimination of surface water. A second weight loss between 100 °C and 150 °C is attributed to the elimination of intercalated water. The third mass loss, in the range of 180–230 °C, is ascribed to the Cd–OH de-hydroxylation. A final mass loss in the range of 280–400 °C is attributed to the Al–OH de-hydroxylation.

The nuclear magnetic resonance (NMR) study of LDHs is highly informative due to the abundance of spin-active nuclei from which site-specific structural information can be deducted. Therefore, ^{27}Al ssNMR measurements are performed to detect any divergence from the expected octahedral coordination of the aluminium elements in the LDH sheets. Fig. S4† shows the ^{27}Al ssNMR spectra of LDHs with different ratios, which reveal one peak at a chemical shift around 15 ppm, proving the octahedral coordination of all the aluminum elements in the layered sheets. Similar spectra are observed for the three different ratios of CdAl LDHs.

The N_2 adsorption–desorption isotherms reveal that all CdAl LDHs exhibit a type IV isotherm with H3 hysteresis loop (Fig. S5†). This is a common signature for nanosheet particles having a wide pore size distribution. The surface area of CdAl LDHs shows an increasing trend as the cationic ratio of the corresponding LDH decreases. The BET surface area obtained for CdAl LDHs with a cationic ratio of 0.33, 0.28 and 0.25 is equal to 46, 59 and 64 $m^2\ g^{-1}$, respectively. The increase of the surface area as the Cd^{2+} content gets higher is attributed to the larger ionic radius of Cd^{2+} (109 Å) in comparison with that of Al^{3+} (67.5 Å).

The synthesized CdAl LDHs exhibit a wide absorption band covering both the UV and visible regions of the electromagnetic spectrum, ranging from 210 nm to 650 nm. The UV-Vis diffuse reflectance spectra of CdAl LDH with different ratios revealed that the intensity of the absorption band in the visible region (around 400 nm) increases as the cationic ratio decreases. Also, the maximum absorption edge is red shifted, which is induced by a decrease of the band gap energy as the Cd^{2+} content in the brucite-like layers increases. The obtained reflectance data is transformed into the Kubelka–Munk model which reveals that the main absorption band is centered at around 398 nm, 402 nm, and 417 nm for a cationic ratio of 0.33, 0.28 and 0.25, respectively (Fig. 2). The bands at 210–240 nm are observed for ligand-to metal charge transfer (LMCT) from the O 2p orbital to the Al 3s and Cd 3d e_g orbitals with a shift towards shorter wavelengths with increasing cationic ratio x.[42–45] The decrease in the band gap energy suggests that less energy is needed for the photodegradation of methylene blue as the cationic ratio decreases.

SEM images of the synthesized LDH with different ratios indicate the self-assembly of all CdAl LDHs into flowery-like microspheres (Fig. 3(A–C)). These spheres show that the material consists of platelets that are connected to each other to form this flowery-like porous structure. Elemental mapping indicates a homogeneous surface distribution of the aluminum and cadmium (Fig. 3(D–F)). 3D electron tomography and virtual

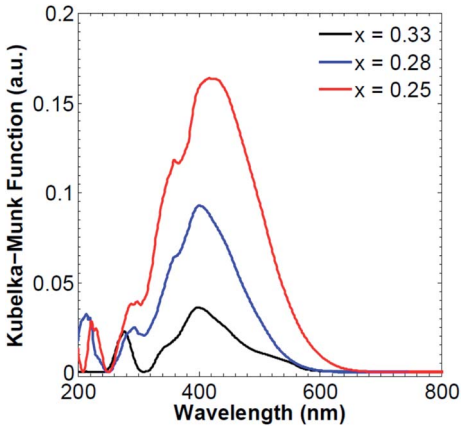

Fig. 2 UV-Vis diffuse reflectance of CdAl LDH with different cationic ratios.

cross-sectional imaging are performed for further investigation of the internal structure of the LDH spheres. 3D reconstruction of the flower-like microspheres proves the void presence in the internal structure of the microspheres (white/gray color in (Fig. 3(G and H))). The virtual cross-sectional cuts reveal that the internal structure consists of inter-connected individual nanosheets which create internal channels and void in the microspheres (Fig. 3(I)).

The chemical state of CdAl LDHs, having different cationic ratios, were examined *via* X-ray photoelectron spectroscopy (XPS). Fig. S6((A)–(C))† shows the overall spectra of the LDHs which reveals the presence of O, Cd and Al peaks indicating the

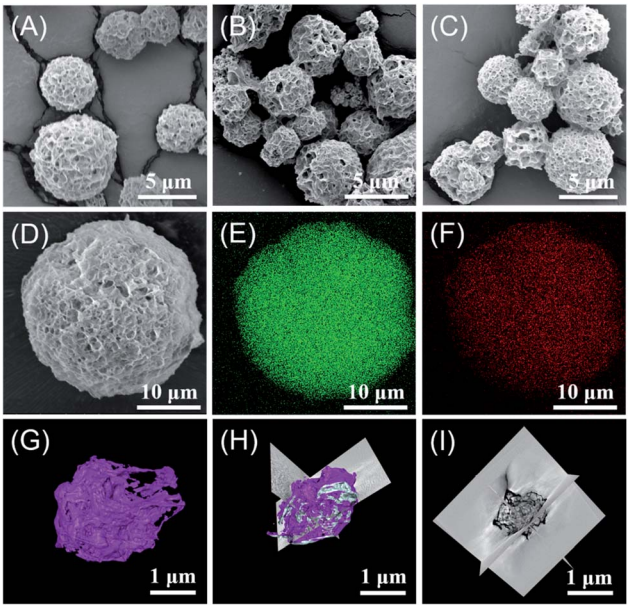

Fig. 3 SEM images of CdAl LDH having $x = 0.33$ (A), $x = 0.28$ (B) and $x = 0.25$ (C). SEM image of CdAl LDH having $x = 0.25$ (D) and its corresponding elemental mapping of aluminum (E) and cadmium (F) using energy dispersive X-ray (EDX) on SEM. 3D tomographic reconstruction (G) and virtual cross-sectional slices along different axes showing the internal microstructure of CdAl LDH with $x = 0.25$ (H and I).

absence of impurities within all samples. Cd 3d core-level spectra reveal two different structures resulting from the spin–orbit splitting of the d orbital into Cd $3d_{3/2}$ (411.9 eV) and Cd $3d_{5/2}$ (404.8 eV) bonding states. Auger electron analysis is performed to differentiate between the Cd(0) and Cd(II) oxidation states of cadmium, revealing the solely presence of Cd^{2+} in all CdAl LDH samples (Fig. S6(E), (I) and (M)).† The binding energy spectra of Al 2p shows one single peak located at 73.7 eV indicating the solely presence of trivalent aluminum cations on the LDH surface. Fig. S6((G), (K) and (O))† shows that the O 1s core-level peak can be deconvoluted into two main peaks located at 531.06 eV and 532.59 eV, which are assigned to O 1s of metal hydroxide M–O–H and H_2O, respectively.

2. Optical properties of CdAl LDH

The electronic and optical absorption behaviour of the prepared LDHs were examined by UV-Vis spectrophotometry. It is seen that the maximum absorption edge is more red shifted as the Cd^{2+} content in the brucite-like layers gradually increases. Besides, according to literature, the optical absorption of LDH near the band-edge can be calculated using the Tauc/Davis–Mott equation: $\alpha\hbar\nu = K(\hbar\nu - E_g)^{n/2}$, where α, $\hbar$, ν, K and E_g are the absorption coefficient, Planck's constant, light frequency, proportionality constant and band gap, respectively.[46] The "n" value represents the characteristics of the transition in CdAl LDH which was determined to be 1, indicating the directly allowed optical transition.[47] The value of E_g is obtained by extrapolating the linear region straight line to the $\hbar\nu$ axis intercept of the $(\alpha\hbar\nu)^2$ *vs.* $\hbar\nu$ plot (Fig. S7†). The band gaps were estimated to be 2.61, 2.53, and 2.35 ev for CdAl LDHs with a cationic ratio of 0.33, 0.28 and 0.25, respectively. Similarly, the DFT calculations revealed a decrease in the band gap for lower cationic ratios of CdAl LDH. The slight increase in the band gap values obtained computationally in comparison to the experimental ones for the same cationic ratio is attributed to the exciton effect.

3. Photocatalytic activity of CdAl LDH

The photocatalytic activity of the prepared samples was evaluated by the degradation of methylene blue solution under visible light irradiation. The rate of methylene blue degradation was recorded with respect to the change in the absorption's intensity at 665 nm. Besides, methylene blue might be reduced to form leucomethylene blue which shows no visible light absorption mainly at 665 nm.[48] In the latter case, a simple decolorization of the dye will be occurring instead of its degradation. To eliminate the possibility of methylene blue decolorization by reduction into the leuco form, the intensity of all the characteristic peaks of methylene blue, located at 250 nm, 290 nm, and 665 nm (Fig. S8†), was recorded over time and showed a decrease in both the aromatic and chromophoric absorbance maxima of MB which suggest a degradation of MB and not a simple decolorization. It is noteworthy that most of the reported photocatalysts, including LDHs, for dye degradation are based on the use of hydrogen peroxide (H_2O_2) to enhance the photocatalytic degradation process. Also, according to literature, many reported the use of catalysts in the photodegradation of organic dyes, including LDHs, along with the use of H_2O_2 which is a key factor that can significantly enhance the decomposition rate of the organic dyes.[49–52] Indeed, H_2O_2 is an electron acceptor which upon irradiation with UV or visible light induces the formation of $OH^{\bullet}$ radicals which itself causes the degradation of the dyes. Yet, in this work, all the subsequent photodegradation experiments were performed in the absence of hydrogen peroxide or any other species that can photo-generate free radicals.

(i). Control experiments. Initially, the control solution, consisting of pure methylene blue (7.5 mg L^{-1}) with no catalyst, was tested under the same experimental conditions and revealed a minimal degradation of methylene blue (10%) over 3 hours (Fig. 4(A), and S8(A)†). Also, the dye adsorption behavior was investigated by stirring it into an individual suspension of each of the synthesized LDHs in dark until a state of adsorption–desorption equilibrium was achieved. The supernatant was collected (1 mL), and its absorbance was measured over time. The methylene blue solution displayed a saturation period of 25 min, 25 min and 40 min for CdAl LDHs with cationic ratios of 0.33, 0.28 and 0.25, respectively (Fig. S9†). Therefore, prior to visible light irradiation, all the prepared LDHs were soaked in the methylene blue solution at dark for 40 min to reach the adsorption equilibrium. Then, we tentatively suggest that any

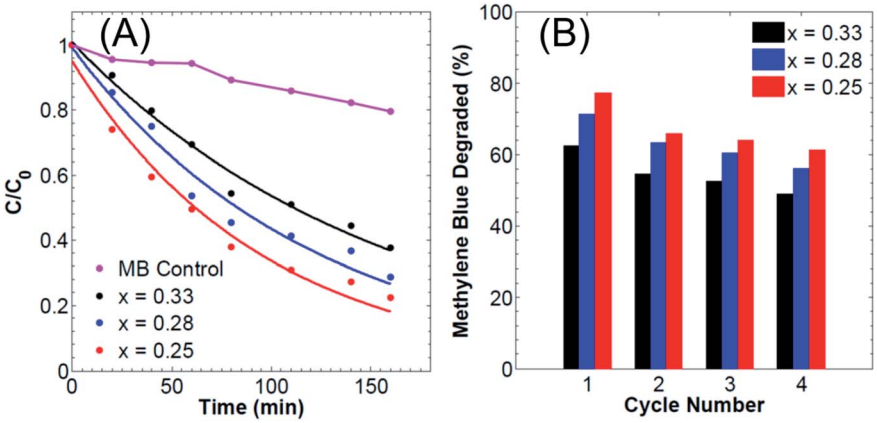

Fig. 4 Photolysis of methylene blue and photocatalytic performance of CdAl LDHs having different cationic ratios in the degradation of methylene blue under visible light (A) and for four consecutive cycles (B).

further decrease in the methylene blue concentration should be assigned to its photocatalytic degradation process by the LDH.

(ii). Catalyst photoactivity, regeneration and stability. The photoassisted degradation of methylene blue using different CdAl LDH catalysts, under same experimental conditions (catalyst loading of 0.6 g L^{-1}; MB concentration of 7.5 mg L^{-1}; pH = 6), is shown in Fig. 4(A). The data revealed that the photodegradation efficiency is inversely proportional to the cationic ratio "*x*" of the LDH where CdAl LDH with $x = 0.25$ displayed the highest photocatalytic activity (78%) and that with $x = 0.33$ exhibited the lowest degradation rate (62%). Note that all the characteristic peaks of methylene blue located at 250 nm, 290 nm, and 665 nm showed a decrease in their intensities indicating its degradation (Fig. S8†). More importantly, the decrease of the peak located at 250 nm indicates the decomposition of the aromatic rings of methylene blue into less harmful non-aromatic sub-products. On the other hand, separate phases of cadmium hydroxide and aluminum hydroxide revealed minimal degradation efficiency of 30% and 25%, respectively (Fig. S10†).

The reusability and stability of CdAl LDH catalysts were carried out for each of the 3 different ratios. After each run, the LDH was separated from the reaction system by centrifugation, washed 4 times with acetone, freeze dried and added into a fresh solution of methylene blue. Fig. 4(B) shows the repetitive photodegradation of methylene blue over 4 cycles for different cationic ratios, with the same dye concentration, catalyst loading and illumination time. The results revealed that the photoactivity of the catalyst remained with a slight decrease (*ca.* 15%) which might be due to the loss of small amount of catalyst during the washing steps. On the other hand, the PXRD and SEM data of the recovered samples, shown in Fig. S11,† reveal the high chemical stability of CdAl LDHs, since both the morphology and the crystal structure of the LDHs were preserved after 4 cycles of photodegradation.

(iii). Investigation of reactive oxygen species. The contribution of reactive oxygen species (ROSs), mainly peroxyl radicals ($O_2^{\bullet -}$), hydroxyl radicals ($OH^{\bullet}$) and singlet oxygen ($^1O_2$), in the photodegradation of methylene blue was investigated using different scavengers. Benzoquinone was used to probe the peroxyl radicals generated during the photodegradation reaction. Fig. 5(A) clearly shows that peroxyl radicals are the main oxidative species that initiates the degradation process upon light irradiation since the degradation was mostly quenched after the addition of benzoquinone. Besides, isopropanol was applied as a scavenger of hydroxyl radicals, which upon addition prevented the degradation of methylene blue but to a lower extent than that of benzoquinone. Lastly, EDTA was employed as a chemical probe to trap singlet oxygen, which represents another important ROS, but it showed a minor prevention in the degradation of the dye. Therefore, it was concluded that the predominant ROS responsible for the decomposition of the dye were the peroxyl radicals (90%), which themselves are responsible for the generation of hydroxyl radicals (35%). Besides, singlet oxygen played a very minor role in the degradation process (10%).

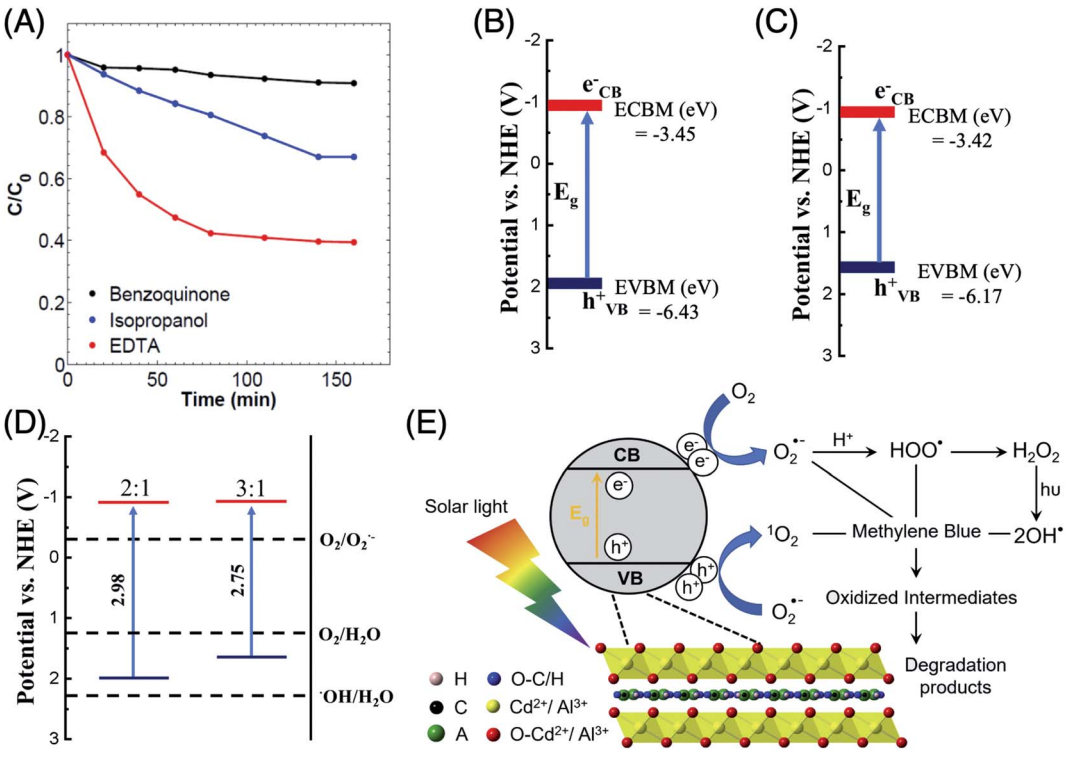

Fig. 5 Photocatalytic performance of CdAl LDH, with a cationic ratio of $x = 0.25$, in the degradation of methylene blue under visible light and in the presence of different reactive oxygen species scavengers (A). Valence and conduction bands potential values *vs.* NHE, obtained using DFT calculations, for CdAl LDHs with cationic ratios of $x = 0.25$ (B) and $x = 0.33$ (C), along with their relative positions in comparison to the potential of some ROS species (D). Schematic representation of the potential photodegradation mechanism (E).

(iv). Mechanism and discussion of visible light photocatalytic reaction using CdAl LDHs with different cationic ratios. The efficiency of photocatalysts depends on both the optical properties and the position of the redox potential in a semiconductor. The redox potential of the donor must be more negative than the valence band position of the semiconductor, and the acceptor molecules should have a more positive potential than the conduction band. From the results of the computational calculations, it was found that the position of the valence and conduction bands of CdAl LDH (Fig. 5(B–D)) suggests that the peroxyl radicals are primarily produced from the reduction of dissolved oxygen by the photogenerated electrons of the conduction band according to eqn (3). Once formed, the peroxyl radicals will either degrade the dissolved methylene blue (eqn (4)) or react with H^+ to generate 2HOO$^\bullet$ which itself will lead to the formation of H_2O_2 (eqn (5)). The photoinduced reduction of H_2O_2 produces OH$^\bullet$ radicals that contribute to the degradation of methylene blue (eqn (6)). The peroxyl radical's oxidation by the photogenerated holes (eqn (7)) leads to the formation of singlet oxygen which contributes to the decomposition process. The degradation mechanism was proposed as follows and summarized in Fig. 5(E):

$$\text{Catalyst} + h\nu \rightarrow \text{Catalyst}\,(e_{\text{conduction band (CD)}}^{-} + h_{\text{valence band (VB)}}^{+}) \quad (1)$$

$$\text{Catalyst}\,(h_{VB}^{+}) + 2H_2O \rightarrow 4H^+ + O_2 \quad (2)$$

$$\text{Catalyst}\,(e_{CD}^{-}) + O_2 \rightarrow \text{Catalyst} + O_2^{\bullet -} \quad (3)$$

$$O_2^{\bullet -} + \text{methylene blue} \rightarrow \text{degradation product} \quad (4)$$

$$2O_2^{\bullet -} + 2H^+ \rightarrow 2HOO^\bullet \rightarrow H_2O_2 \quad (5)$$

$$H_2O_2 + h\nu \rightarrow 2OH^\bullet + \text{methylene blue} \rightarrow \text{degradation product} \quad (6)$$

$$\text{Catalyst}\,(h_{VB}^{+}) + O_2^{\bullet -} \rightarrow \text{Catalyst} + {}^1O_2 \quad (7)$$

$${}^1O_2 + \text{methylene blue} \rightarrow \text{degradation product} \quad (8)$$

Besides, the total density of states (TDOS) and the partial density of states (PDOS) for CdAl LDH with cationic ratios of 0.33 and 0.25 are presented in Fig. 6. The O 2p and Cl 2p orbitals are shown to be the main contributors to the front of the VB indicating that the photogenerated holes are located on the oxygen and chloride atoms. The holes on the oxygen atoms of the brucite-like sheets oxidize the adsorbed water molecules

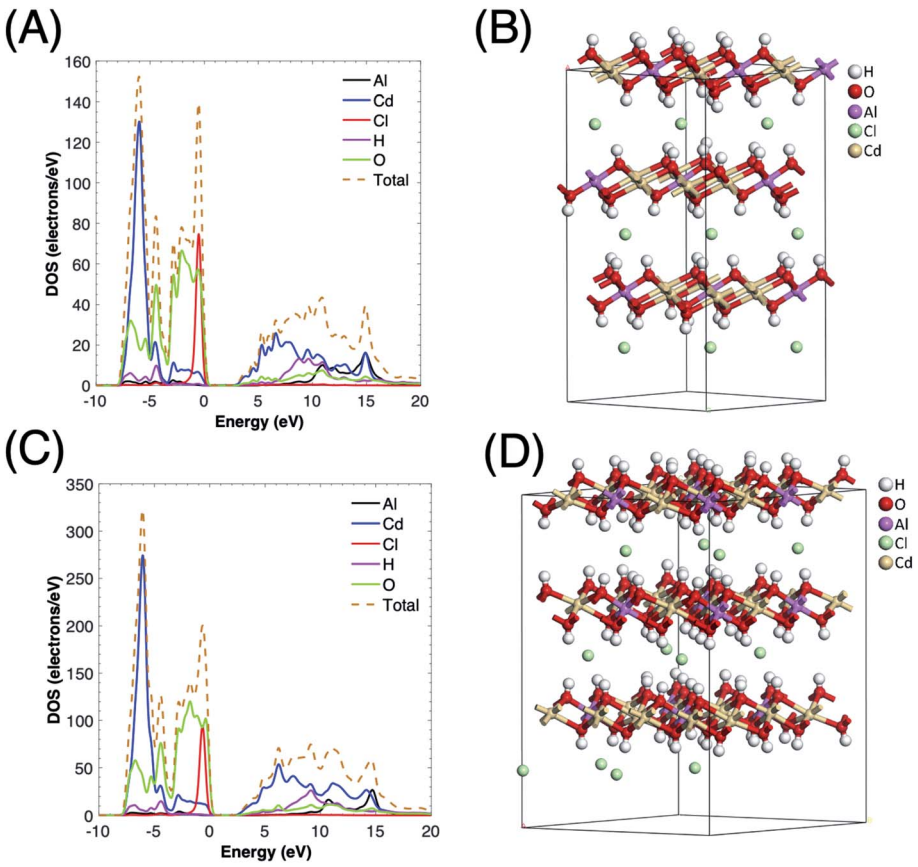

Fig. 6 Total and partial density of states for CdAl LDH with cationic ratio of $x = 0.33$ (A) and $x = 0.25$ (C) along with the optimized crystal structures for $x = 0.33$ (B) and $x = 0.25$ (D). Different supercell sizes were used ($4 \times 4 \times 1$ for $x = 0.33$ (B) and $3 \times 3 \times 1$ for $x = 0.25$ (D)) for different cationic ratios as DFT calculation requires fully occupied atomic sites.

into O_2. On the other hand, the photogenerated holes on the interlayer chloride anions tend to recombine since they show minor interactions with the intercalated water molecules. The frontier of the CB is mainly composed of Cd 3d orbitals where the photogenerated electrons are localized, whereas the contribution of the aluminum cations is negligible, as shown in the PDOS data. Also, as the cationic ratio of CdAl LDH decreases, the required amount of interlayer anions, which are necessary to restore the electroneutrality of LDH, will decrease. Therefore, the decrease in cationic ratio will generate both a higher contribution to the CB and a lower recombination rate which enhance the photocatalytic activity.

D. Conclusions

CdAl LDHs with different cationic ratios were synthesized by the reaction-diffusion method. UV-Vis diffuse reflectance measurements confirmed that all LDHs showed a broad absorption band in the visible light region. The prepared LDHs were demonstrated to be highly efficient for the photodegradation of methylene blue using visible light and in the absence of hydrogen peroxide. The photoactivity of CdAl LDH revealed a strong dependence on the cationic ratio of the LDH where the Cd^{2+} ions present in the CdO_6 octahedrons of the CdAl brucite-like sheets played an important role in both the absorption of visible light and the decrease of the band gap. A proposed mechanism for methylene blue degradation, which was supported by DFT calculations, was put forward by which the contribution of different reactive oxygen species played a crucial role.

Conflicts of interest

There are no conflicts to declare.

Acknowledgements

MAG acknowledges the support of the Arab Fund Fellowship Program. The authors thankfully acknowledge the funding provided by the American University of Beirut Research Board and by the Lebanese National Council for Scientific Research (LCNSR). We also thank Dr Rashid Sougrat at King Abdullah University of Science and Technology for his assistance in the 3D tomography measurements.

References

1 C. Karunakaran, R. Dhanalakshmi, P. Gomathisankar and G. Manikandan, *J. Hazard Mater.*, 2010, **176**, 799–806.
2 Y. Guo, S. Chu, S. Yan, Y. Wang and Z. Zou, *Chem. Commun.*, 2010, **46**, 7325–7327.
3 S. Liu, H. Sun, S. Liu and S. Wang, *Chem. Eng. J.*, 2013, **214**, 298–303.
4 C. Lizama, J. Freer, J. Baeza and H. D. Mansilla, *Catal. Today*, 2002, **76**, 235–246.
5 X. Xu, R. Lu, X. Zhao, S. Xu, X. Lei, F. Zhang and D. G. Evans, *Appl. Catal., B*, 2011, **102**, 147–156.
6 J. Bedia, V. Muelas-Ramos, M. Peñas-Garzón, A. Gómez-Avilés, J. Rodríguez and C. Belver, *Catalysts*, 2019, **9**, 52.
7 X. Zhang, A. J. Du, P. Lee, D. D. Sun and J. O. Leckie, *J. Membr. Sci.*, 2008, **313**, 44–51.
8 S. M. Jung and P. Grange, *Appl. Catal., B*, 2001, **32**, 123–131.
9 K. G. Laurier, F. Vermoortele, R. Ameloot, D. E. De Vos, J. Hofkens and M. B. Roeffaers, *J. Am. Chem. Soc.*, 2013, **135**, 14488–14491.
10 M.-Q. Yang, C. Han and Y.-J. Xu, *J. Phys. Chem. C*, 2015, **119**, 27234–27246.
11 A. Mantilla, F. Tzompantzi, J. Fernández, J. D. Góngora, G. Mendoza and R. Gómez, *Catal. Today*, 2009, **148**, 119–123.
12 W.-K. Jo, Y.-G. Kim and S. Tonda, *J. Hazard Mater.*, 2018, **357**, 19–29.
13 D. Saliba, A. Ezzeddine, A.-H. Emwas, N. M. Khashab and M. Al-Ghoul, *Cryst. Growth Des.*, 2016, **16**, 4327–4335.
14 Q. Wang and D. O'Hare, *Chem. Rev.*, 2012, **112**, 4124–4155.
15 J. Yu, Q. Wang, D. O'Hare and L. Sun, *Chem. Soc. Rev.*, 2017, **46**, 5950–5974.
16 L. Mohapatra and K. Parida, *J. Mater. Chem. A*, 2016, **4**, 10744–10766.
17 J. Liu and G. Zhang, *Phys. Chem. Chem. Phys.*, 2014, **16**, 8178–8192.
18 L. Mohapatra and K. Parida, *Sep. Purif. Technol.*, 2012, **91**, 73–80.
19 N. Ahmed, M. Morikawa and Y. Izumi, *Catal. Today*, 2012, **185**, 263–269.
20 D. Saliba, A. Ezzeddine, R. Sougrat, N. M. Khashab, M. Hmadeh and M. Al-Ghoul, *ChemSusChem*, 2016, **9**, 800–805.
21 Z. Wang, S. Zeng, W. Liu, X. Wang, Q. Li, Z. Zhao and F. Geng, *ACS Appl. Mater. Interfaces*, 2017, **9**, 1488–1495.
22 K. Yan, T. Lafleur, J. Chai and C. Jarvis, *Electrochem. Commun.*, 2016, **62**, 24–28.
23 Y. Fu, F. Ning, S. Xu, H. An, M. Shao and M. Wei, *J. Mater. Chem. A*, 2016, **4**, 3907–3913.
24 G. Huang, J. Chen, D. Wang, Y. Sun, L. Jiang, Y. Yu, S. Ma and Y. Kang, *Mater. Lett.*, 2016, **173**, 227–230.
25 S. Xia, M. Shao, X. Zhou, G. Pan and Z. Ni, *J. Mol. Catal. A: Chem.*, 2015, **406**, 127–136.
26 S. Xia, X. Zhang, X. Zhou, Y. Meng, J. Xue and Z. Ni, *Appl. Catal., B*, 2017, **214**, 78–88.
27 G. Zhang, X. Zhang, Y. Meng, G. Pan, Z. Ni and S. Xia, *Chem. Eng. J.*, 2020, **392**, 123684.
28 J. Xue, T. Chen, Y. Meng, X. Zhou, G. Pan, Z. Ni and S. Xia, *J. Photochem. Photobiol., A*, 2019, **371**, 33–43.
29 Y. Meng, S. Xia, G. Pan, J. Xue, J. Jiang and Z. Ni, *Korean J. Chem. Eng.*, 2017, **34**, 2331–2341.
30 D. Gao, H. Yu and Y. Xu, *Appl. Surf. Sci.*, 2018, **462**, 623–632.
31 N. A. Bakar, N. Jamil, W. Tan, N. Sabri, T.-W. Tan and M. A. Bakar, *J. Photochem. Photobiol., A*, 2018, **352**, 9–18.
32 S. Xia, L. Zhang, G. Pan, P. Qian and Z. Ni, *Phys. Chem. Chem. Phys.*, 2015, **17**, 5345–5351.
33 Z. Gu, J. J. Atherton and Z. P. Xu, *Chem. Commun.*, 2015, **51**, 3024–3036.
34 M. Li, J. Cheng, J. Fang, Y. Yang, F. Liu and X. Zhang, *Electrochim. Acta*, 2014, **134**, 309–318.

35 J. J. Bravo-Suárez, E. A. Páez-Mozo and S. T. Oyama, *Quim. Nova*, 2004, **27**, 601–614.
36 D. Saliba, M. Ammar, M. Rammal, M. Al-Ghoul and M. Hmadeh, *J. Am. Chem. Soc.*, 2018, **140**, 1812–1823.
37 D. Saliba and M. Al-Ghoul, *CrystEngComm*, 2016, **18**, 8445–8453.
38 K. Parida, N. Baliarsingh, B. S. Patra and J. Das, *J. Mol. Catal. A: Chem.*, 2007, **267**, 202–208.
39 F. Van Laar, D. E. De Vos, F. Pierard, A. Kirsch-De Mesmaeker, L. Fiermans and P. Jacobs, *J. Catal.*, 2001, **197**, 139–150.
40 A. A. Jelle, M. Hmadeh, P. G. O'Brien, D. D. Perovic and G. A. Ozin, *ChemNanoMat*, 2016, **2**, 1047–1054.
41 A. V Radha, P. Vishnu Kamath and C. Shivakumara, *Order and disorder among the layered double hydroxides: combined Rietveld and DIFFaX approach*, 2007.
42 D. P. Sahoo, S. Nayak, K. H. Reddy, S. Martha and K. Parida, *Inorg. Chem.*, 2018, **57**, 3840–3854.
43 B. Tyagi, U. Sharma and R. V. Jasra, *Appl. Catal., A*, 2011, **408**, 171–177.
44 A. A. A. Ahmed, Z. A. Talib, M. Z. bin Hussein and A. Zakaria, *J. Solid State Chem.*, 2012, **191**, 271–278.
45 H. Chai, X. Xu, Y. Lin, D. G. Evans and D. Li, *Polym. Degrad. Stabil.*, 2009, **94**, 744–749.
46 K. Parida and L. Mohapatra, *Chem. Eng. J.*, 2012, **179**, 131–139.
47 J. Luan, Z. Zou, M. Lu, G. Luan and Y. Chen, *Res. Chem. Intermed.*, 2006, **32**, 31–42.
48 S.-K. Lee and A. Mills, *Chem. Commun.*, 2003, 2366–2367.
49 A. Jawad, X. Lu, Z. Chen and G. Yin, *J. Phys. Chem. A*, 2014, **118**, 10028–10035.
50 X. Tang and Y. Liu, *Dyes Pigm.*, 2016, **134**, 397–408.
51 J. Bai, Y. Liu, X. Yin, H. Duan and J. Ma, *Appl. Surf. Sci.*, 2017, **416**, 45–50.
52 C. C. Pei and W. Chu, *Chem. Eng. J.*, 2013, **223**, 665–669.